Comparative study of current-mode controllers for the positive output elementary Luo converter via state-space and frequency response approaches

Chincholkar S.H.[1], and Chok-You Chan[2]

School of Electrical and Electronic Engineering
South Spine, Block S2.1
Nanyang Technological University
50 Nanyang Avenue
Singapore 639798.
[1]Email: saty0007@e.ntu.edu.sg
[2] Email: ecychan@ntu.edu.sg

Abstract*:* This paper presents the comparative study of dual-loop current-mode controllers to achieve the output voltage regulation of the positive output elementary Luo (POEL) converter. The POEL converter is a fourth order dc-dc boost converter developed using the voltage lift technique that gives a positive load voltage. Two current-mode controllers, one using the input inductor current and one using the output inductor current, are studied. Both state-space and frequency response approaches are used in the study to obtain a better insight of the comparative study. It is demonstrated that the controller using the input inductor current is more suitable for the regulation of the POEL converter. Experimental Results showing the features of the controller in the presence of load and reference voltage changes are also provided to validate the theoretical conclusions.

1 Introduction

With the development of new technologies in various applications such as medical equipment design, renewable energy power systems, defense equipment, power supplies, etc, dc-dc converters with low ripples in the voltage and current, high efficiency and simple architecture are employed in order to achieve the precise output voltage regulation against parameter, line and load disturbances [1-3]. For example, the outputs of most of the renewable energy sources like solar arrays and fuel cells are very low and DC-DC converters are employed to connect to the grid or battery pack [4-6]. One of these converters is the positive output elementary Luo converters which are based on the voltage-lift technique [7-8]. As compared to the other topologies used in dc-dc conversion (step-up), Luo converters differs in the sense of constructional architecture which is of fourth order type architecture with a single active switch [9-11]. The other characteristic feature of the Luo converter is its reduced ripple in both output voltage and current as compared to the conventional boost converter [12-13].

There have been some works done on the modelling and control of the POEL converter [14-15]. Most of them are on the sliding mode control of the converter. There are four variables in the fourth-order POEL converter. However, invariably, only the input inductor current and the output voltage were chosen for feedback purposes. Why were they chosen is not explained. Since there are more variables to consider as compared to the conventional boost converter, the question is: Which are the suitable variables for feedback purposes? There has not been much study on this aspect when designing low-order controllers for high-order converters. The controllers should be of low order for ease of design and implementation. This area is growing in importance as most boost converters providing wide conversion ratios are of higher-order and thus more difficult to control.

The current-mode control has been widely used to regulate the output voltage of dc-dc converters. Basically it is a two-loop control using the inductor current in the inner-loop to

maximize the system bandwidth and using the output voltage in the outer loop to provide the reference value for the current loop. Its advantages over the traditional single-loop voltage mode control are improved dynamic performance, i.e., fast and robust output response as well as improved closed loop bandwidth [17-19]. While current-mode control has been applied to different types of converters for the regulation of the output voltage, for example [20-22], there are very few works reported (e.g., [16]) on the comparative study of current-mode controllers using different inductor currents for feedback purposes.

In this paper, a comparative study of two current-mode controllers (using input and the output inductor currents) for the regulation of the POEL converter is presented. To get a better insight in the study, both state-space and frequency response approaches were used. The comparative study in [16] for a fifth-order dc-dc boost converter shows that controller using the output inductor current is the most suitable for feedback purpose. However, in the present study, the controller using the input inductor current is the most suitable for regulating the POEL converter. The results are borne out by numerical studies.

The paper is organized as follows. Section 2 presents the average state-space model of the POEL converter and its equilibrium values. The analyses of the current-controlled system using the state-space and frequency response approaches are given in Sections 3 and 4, respectively. The experimental results showing the features of the current-mode controller in the presence of load and reference voltage changes are given in section 5.

2 Average model of the POEL converter

Fig. 1 shows the circuit diagram of the POEL converter. The average state space model of the POEL converter operating in the continuous mode is described as follows [14, 15]:

$$\frac{di_{L_1}}{dt} = -\frac{1-k}{L_1} v_{C_1} + \frac{kE}{L_1} \tag{1}$$

$$\frac{dv_{C_1}}{dt} = \frac{1-k}{C_1} i_{L_1} - \frac{k}{C_1} i_{L_2} \tag{2}$$

$$\frac{di_{L_2}}{dt} = \frac{k}{L_2} v_{C_1} - \frac{1}{L_2} v_{C_2} + \frac{kE}{L_2} \tag{3}$$

$$\frac{dv_o}{dt} = \frac{1}{C_2} i_{L_2} - \frac{1}{RC_2} v_o \tag{4}$$

where i_{L_1}, i_{L_2}, v_{C_1} and $v_{C_2} = v_o$ are the average current of inductor L_1, average current of inductor L_2, average voltage of capacitor C_1 and average voltage of capacitor C_2, respectively. The scalar k denotes the duty ratio, where $0 \leq k \leq 1$. From (1) – (4), the following equilibrium values are obtained:

$$I_{L_1} = \frac{V_o^2}{RE}, \quad I_{L_2} = \frac{V_o}{R}, \quad V_{C_1} = V_{C_2} = V_o, \quad \frac{V_o}{E} = \frac{K}{1-K}, \quad K = \frac{V_o}{E+V_o} \tag{5}$$

where I_{L_1}, I_{L_2}, V_{C_1}, $V_{C_2} = V_o$ and K are the equilibrium values of i_{L_1}, i_{L_2}, v_{C_1}, v_o and k, respectively. If the desired value of v_o is V_d, then

$$I_{L_1} = \frac{V_d^2}{RE}, \quad I_{L_2} = \frac{V_d}{R}, \quad V_{C_1} = V_d, \quad \frac{V_d}{E} = \frac{K}{1-K}, \quad K = \frac{V_d}{E+V_d} \tag{6}$$

The problem at hand is to find a suitable current mode controller to regulate the output voltage of the POEL converter in the presence of uncertain load.

3 Comparison of controllers using state-space approach

In this section, the current mode controllers using the input and output inductor currents are studied and compared. The controller using the input inductor current will be studied first and then followed by the controller using the output inductor current.

3.1 Controller using input inductor current

The current mode controller using the input inductor current is described as:

$$k = K - K_{P1}\left(i_{L_1} - i_{L_{1ref}}\right) - K_{I1} \int (v_o(\tau) - V_d)\, d\tau \tag{7}$$

where K_{P1}, $K_{I1} > 0$. Define the errors as follows:

$$e_1 = i_{L_1} - \frac{V_d^2}{RE}, \quad e_2 = v_{C_1} - V_d, \quad e_3 = i_{L_2} - \frac{V_d}{R}, \quad e_4 = v_o - V_d \tag{8}$$

Substituting (7) – (8) into (1) – (4) and using (6) yield the following set of equations:

$$\dot{e}_1 = -\frac{1}{L_1}\left(\frac{E}{V_d+E} + K_{P1}e_1 + \sigma\right)(e_2 + V_d) + \frac{E}{L_1}\left(\frac{V_d}{V_d+E} - K_{P1}e_1 - \sigma\right) \tag{9}$$

$$\dot{e}_2 = \frac{1}{C_1}\left(\frac{E}{V_d+E} + K_{P1}e_1 + \sigma\right)\left(e_1 + \frac{V_d^2}{RE}\right) - \frac{1}{C_1}\left(\frac{V_d}{V_d+E} - K_{P1}e_1 - \sigma\right)\left(e_3 + \frac{V_d}{R}\right) \tag{10}$$

$$\dot{e}_3 = \frac{1}{L_2}\left(\frac{V_d}{V_d+E} - K_{P1}e_1 - \sigma\right)(e_2 + V_d + E) - \frac{1}{L_2}(e_4 + V_d) \tag{11}$$

$$\dot{e}_4 = \frac{1}{C_2}\left(e_3 + \frac{V_d}{R}\right) - \frac{1}{RC_2}(e_4 + V_d) \tag{12}$$

$$\dot{\sigma} = K_{I1}e_4 \tag{13}$$

The unique equilibrium point of (9) – (13) is given by

$$(e_{1\infty}, e_{2\infty}, e_{e\infty}, e_{4\infty}, \sigma_\infty) = (0,\ 0,\ 0,\ 0, 0) \tag{14}$$

Linearizing (9) – (13) about equilibrium point gives the following system [23]:

$$\dot{\boldsymbol{z}} = \boldsymbol{M}\boldsymbol{z} \tag{15}$$

where $\boldsymbol{z} = [z_1\ z_2\ z_3\ z_4\ z_5]^T$, and

$$z_1 = e_1 - e_{1\infty},\ z_2 = e_2 - e_{2\infty},\ z_3 = e_3 - e_{3\infty},\ z_4 = e_4 - e_{4\infty},\quad z_5 = \sigma - \sigma_\infty$$

$$\boldsymbol{M} = \begin{bmatrix} -\frac{K_{P1}(V_d+E)}{L_1} & -\frac{E}{L_1(V_d+E)} & 0 & 0 & -\frac{V_d+E}{L_1} \\ \frac{E}{C_1(V_d+E)} + \frac{K_{P1}V_d}{RC_1}\left(\frac{V_d}{E}+1\right) & 0 & -\frac{V_d}{C_1(V_d+E)} & 0 & \frac{V_d}{RC_1}\left(\frac{V_d}{E}+1\right) \\ -\frac{K_{P1}(V_d+E)}{L_2} & \frac{V_d}{L_2(V_d+E)} & 0 & -\frac{1}{L_2} & -\frac{(V_d+E)}{L_2} \\ 0 & 0 & \frac{1}{C_2} & -\frac{1}{RC_2} & 0 \\ 0 & 0 & 0 & K_{I1} & 0 \end{bmatrix}$$

The system (15) will be stable if the eigenvalues of $\boldsymbol{M}$, i.e., the roots of $|s\boldsymbol{I} - \boldsymbol{M}| = 0$, where *s* is a complex variable, all lie in the open left-half complex plane. The root locus method can be used to analyze system stability [24]. This is illustrated as follows.

Consider the POEL converter with following circuit parameter values:

$E = 12V,\ V_d = 18V,\ L_1 = 1mH,\ L_2 = 10mH,\ C_1 = 47\mu F,\ C_2 = 100\mu F,\ R = 22\ \Omega$

The characteristic polynomial $|s\boldsymbol{I} - \boldsymbol{M}|$ is thus given by

$$|s\boldsymbol{I} - \boldsymbol{M}| = s^5 + (30000K_{P1} + 454.54)\, s^4 + (3.1 \times 10^7 K_{P1} + 5.16 \times 10^6)\, s^3 + (7.62 \times 10^{10} K_{P1} + 3 \times 10^7 K_{I1} + 1.89 \times 10^9)\, s^2 + (3.48 \times 10^{13} K_{P1} - 2.61 \times 10^{10} K_{I1} + 3.4 \times 10^{12})\, s + 2.55 \times 10^{14} K_{I1}$$

Fig. 2a shows the root locus plot for $K_{P1} = 0.08$, $0 < K_{I1} < 12$. The arrows show the poles are moving from $K_{I1} = 0$. The system is stable for all values of K_{I1} in this range.

3.2 Controller using output inductor current

The controller using the output inductor current assumes the following form:

$$k = K - K_{P2}\left(i_{L_2} - i_{L_{2ref}}\right) - K_{I2}\int (v_0(\tau) - V_d)\, d\tau \tag{16}$$

where K_{P2}, $K_{I2} > 0$. Substituting (8) and (16) into (1) – (4) and using (6) yields the following error dynamics:

$$\dot{e}_1 = -\frac{1}{L_1}\left(\frac{E}{V_d+E} + K_{P2}e_3 + \sigma\right)(e_2 + V_d) + \frac{E}{L_1}\left(\frac{V_d}{V_d+E} - K_{P2}e_3 - \sigma\right) \tag{17}$$

$$\dot{e}_2 = \frac{1}{C_1}\left(\frac{E}{V_d+E} + K_{P2}e_3 + \sigma\right)\left(e_1 + \frac{V_d^2}{RE}\right) - \frac{1}{C_1}\left(\frac{V_d}{V_d+E} - K_{P2}e_3 - \sigma\right)\left(e_3 + \frac{V_d}{R}\right) \tag{18}$$

$$\dot{e}_3 = \frac{1}{L_2}\left(\frac{V_d}{V_d+E} - K_{P2}e_3 - \sigma\right)(e_2 + V_d + E) - \frac{1}{L_2}(e_4 + V_d) \tag{19}$$

$$\dot{e}_4 = \frac{1}{C_2}\left(e_3 + \frac{V_d}{R}\right) - \frac{1}{RC_2}(e_4 + V_d) \tag{20}$$

$$\dot{\sigma} = K_{I2}e_4 \tag{21}$$

The unique equilibrium point of (17) – (21) is $(e_{1\infty}, e_{2\infty}, e_{e\infty}, e_{4\infty}, \sigma_\infty) = (0, 0, 0, 0, 0)$. Linearization of (17) – (21) about this equilibrium point yields the system of the form:

$$\dot{\boldsymbol{z}} = \boldsymbol{N}\boldsymbol{z} \tag{22}$$

where

$$\boldsymbol{N} = \begin{bmatrix} 0 & -\frac{E}{L_1(V_d+E)} & -\frac{K_{P2}(V_d+E)}{L_1} & 0 & -\frac{V_d+E}{L_1} \\ \frac{E}{C_1(V_d+E)} & 0 & -\frac{V_d}{C_1(V_d+E)} + \frac{K_{P2}V_d}{RC_1}\left(\frac{V_d}{E}+1\right) & 0 & \frac{V_d}{RC_1}\left(\frac{V_d}{E}+1\right) \\ 0 & \frac{V_d}{L_2(V_d+E)} & -\frac{K_{P2}(V_d+E)}{L_2} & -\frac{1}{L_2} & -\frac{(V_d+E)}{L_2} \\ 0 & 0 & \frac{1}{C_2} & -\frac{1}{RC_2} & 0 \\ 0 & 0 & 0 & K_{I2} & 0 \end{bmatrix}$$

For the same set of circuit parameter values that were used for the controller using the input inductor current, the characteristic polynomial $|s\boldsymbol{I} - \boldsymbol{N}|$ is given by:

$$|s\boldsymbol{I} - \boldsymbol{N}| = s^5 + (3000K_{P2} + 454.54)\, s^4 + (5.17 \times 10^6 - 1.24 \times 10^6 K_{P2})\, s^3 + (2.43 \times 10^{10} K_{P2} + 3 \times 10^7 K_{I2} + 1.89 \times 10^9)\, s^2 + (1.16 \times 10^{13} K_{P2} - 2.61 \times 10^{10} K_{I2} + 3.40 \times 10^{12})\, s + 2.55 \times 10^{14} K_{I2}$$

Fig. 2b shows the root locus plot for $K_{P2} = 0.08$, $0 < K_{I2} < 12$. It is seen that even for small values of K_{I2}, there are poles in the right-half complex plane, i.e., the system is unstable. As such, the controller using the input inductor current should be used. This confirms why it is the preferred variable for feedback purposes.

4 Comparison of controllers using frequency response approach

In section 3, the current-mode controllers using the input and output inductor currents were studied using the state-space approach. In this section, the controllers are studied using another approach, the frequency response approach, to help give a better insight into the comparative study.

4.1 Small Signal model and Transfer functions

To facilitate the comparative study using the above approach, the small signal model is first derived for the POEL converter by linearizing (1) – (4) around the equilibrium values (6) and then introducing small ac perturbations. The model obtained is described as:

$$\dot{\tilde{\boldsymbol{x}}} = \boldsymbol{a}\tilde{\boldsymbol{x}} + \boldsymbol{b}\tilde{u} + \boldsymbol{m}\tilde{k} \tag{23a}$$

$$\tilde{y} = \boldsymbol{c}\tilde{\boldsymbol{x}} \tag{23b}$$

where $\tilde{k}$ represents small signal variations in duty cycle k i.e. $k = K + \tilde{k}$ and $\tilde{x}$ represents the small signal variations in state variables such that $\tilde{\boldsymbol{x}} = [\tilde{\imath}_{L_1} \tilde{v}_{c1}\ \tilde{\imath}_{L_2}\ \tilde{v}_{c2}\ ]$ and $\tilde{u} = [\ \tilde{v}_{in}\ ]$. Matrices $\boldsymbol{a}, \boldsymbol{b}, \boldsymbol{m}$ and $\boldsymbol{c}$ are given by

$$\boldsymbol{a} = \begin{bmatrix} 0 & -\frac{K'}{L_1} & 0 & 0 \\ \frac{K'}{C_1} & 0 & -\frac{K}{C_1} & 0 \\ 0 & \frac{K}{L_2} & 0 & -\frac{1}{L_2} \\ 0 & 0 & \frac{1}{C_2} & -\frac{1}{RC_2} \end{bmatrix},\ \boldsymbol{b} = \begin{bmatrix} \frac{K}{L_1} \\ 0 \\ \frac{K}{L_2} \\ 0 \end{bmatrix},\ \boldsymbol{m} = \begin{bmatrix} \frac{V_{C1}+V_{in}}{L_1} \\ -\frac{I_{L1}+I_{L2}}{C_1} \\ \frac{V_{c1}+V_{in}}{L_2} \\ 0 \end{bmatrix},\ \boldsymbol{c} = \begin{bmatrix} 1 & 0 & 0 & 0 \\ 0 & 0 & 1 & 0 \\ 0 & 0 & 0 & 1 \end{bmatrix}$$

where $K' = 1 - K$ and V_{C1}, I_{L1} and I_{L2} represent the steady-state values of the capacitor voltage and the currents flowing in inductors L_1 and L_2, respectively.

The transfer functions required can now be obtained easily from the state space model and are given as follows:

$$G_1(s) = \frac{\tilde{\imath}_{L_1}(s)}{\tilde{k}(s)} = \frac{q_{1(s)}}{p(s)} = \frac{a_0 s^3 + a_1 s^2 + a_2 s + a_3}{s^4 + d_0 s^3 + d_1 s^2 + d_2 s + d_3} \tag{24}$$

$$G_2(s) = \frac{\tilde{\imath}_{L_2}(s)}{\tilde{k}(s)} = \frac{q_1'(s)}{p(s)} = \frac{b_0 s^3 + b_1 s^2 + b_2 s + b_3}{s^4 + d_0 s^3 + d_1 s^2 + d_2 s + d_3} \tag{25}$$

$$G_3(s) = \frac{\tilde{v}_0(s)}{\tilde{k}(s)} = \frac{q_2(s)}{p(s)} = \frac{c_1 s^2 + c_2 s + c_3}{s^4 + d_0 s^3 + d_1 s^2 + d_2 s + d_3} \tag{26}$$

where the small ac perturbations are represented by "~" and

$$a_0 = \frac{(E+V_d)}{L_1},\quad a_1 = \frac{(1-K)(I_{L_1}+I_{L_2})}{C_1 L_1} + \frac{(E+V_d)}{C_2 L_1 R},$$

$$a_2 = \frac{(1-K)(I_{L_1}+I_{L_2})}{C_1 C_2 L_1 R} + \frac{(E+V_d)}{L_1 L_2}\left(\frac{1}{C_2} + \frac{K}{C_1}\right),\quad a_3 = \frac{(1-K)(I_{L_1}+I_{L_2})}{C_1 C_2 L_1 L_2} + \frac{K(E+V_d)}{C_1 C_2 L_1 L_2 R},$$

$$b_0 = \frac{(E+V_d)}{L_2},\quad b_1 = -\frac{K(I_{L_1}+I_{L_2})}{C_1 L_2} + \frac{(E+V_d)}{C_2 L_2 R},\quad b_2 = -\frac{K(I_{L_1}+I_{L_2})}{C_1 C_2 L_2 R} + \frac{(E+V_d)(1-K)}{C_1 L_1 L_2}, \tag{27}$$

$$b_3 = \frac{(E+V_d)(1-K)}{C_1 C_2 L_1 L_2 R},\quad c_1 = \frac{(E+V_d)}{C_2 L_2},\quad c_2 = -\frac{K(I_{L_1}+I_{L_2})}{C_1 C_2 L_2},\quad c_3 = \frac{(E+V_d)(1-K)}{C_1 C_2 L_1 L_2},$$

$d_0 = \frac{1}{C_2 R}$, $d_1 = \frac{(1-K)^2}{C_1 L_1} + \frac{1}{L_2}\left(\frac{1}{C_2} + \frac{K^2}{C_1}\right)$, $d_2 = \frac{(1-K)^2}{C_1 C_2 L_1 R} + \frac{K^2}{C_1 C_2 L_2 R}$,

$d_3 = \frac{(1-K)^2}{C_1 C_2 L_1 L_2}$

Using the same set of circuit parameter values that were used in Section 3, the following transfer functions are obtained:

$$G_1(s) = \frac{\tilde{\imath}_{L_1}(s)}{\tilde{k}(s)} = \frac{q_{1(s)}}{p(s)} = \frac{3x10^4\, s^3 + 3.104x10^7\, s^2 + 7.621x10^{10}\, s + 3.482x10^{13}}{s^4 + 454.5\, s^3 + 5.17x10^6\, s^2 + 1.896x10^9\, s + 3.4042x10^{12}} \quad (28)$$

$$G_2(s) = \frac{\tilde{\imath}_{L_2}(s)}{\tilde{k}(s)} = \frac{q_1{}'(s)}{p(s)} \frac{3000\, s^3 - 1.248x10^6\, s^2 + 2.434x10^{10}\, s + 1.161x10^{13}}{s^4 + 454.5\, s^3 + 5.17x10^6\, s^2 + 1.896x10^9\, s + 3.404x10^{12}} \quad (29)$$

$$G_3(s) = \frac{\tilde{v}_0(s)}{\tilde{k}(s)} = \frac{q_2(s)}{p(s)} \frac{3x10^7\, s^2 - 2.611x10^{10}\, s + 2.553x10^{14}}{s^4 + 454.5\, s^3 + 5.17x10^6\, s^2 + 1.896x10^9\, s + 3.404x10^{12}} \quad (30)$$

It is seen that the transfer function $G_3(s)$ has non-minimum phase characteristics due to the presence of zeros in the right-half complex plane (negative coefficient in the numerator). Thus, it becomes very difficult to design a controller for the regulation of the output voltage using a single loop since the resonance peak presents abrupt changes in the phase (see Fig. 3a). The use of a multi-loop control scheme thus becomes necessary in order to minimize the effects of the resonance peak and to increase the bandwidth [25]. The multi-loop scheme is shown in Fig. 4.

4.2 Controller design using input inductor current

As mentioned earlier, the current loop is mainly designed to minimize the resonance peak present in $G_3(s) = \tilde{v}_0(s)/\tilde{k}(s)$. After introducing the current controller $G_c(s) = K_P$ in the controller scheme shown in Fig. 4, the transfer function $G_{ic}(s) = \tilde{v}_0(s)/\tilde{\imath}_{L1ref}(s)$ is given by (see Fig. 4)

$$G_{ic}(s) = \frac{\tilde{v}_0(s)}{\tilde{\imath}_{L1ref}(s)} = \frac{\frac{1}{V_p} * G_c(s) * G_1(s)}{1 + \frac{1}{V_p} * G_c(s) * G_1(s) * N} * \frac{G_3(s)}{G_1(s)} \quad (31)$$

From (24) and (26) and Fig. 4, $G_{ic}(s)$ can be obtained as

$$G_{ic}(s) = \frac{\tilde{v}_0(s)}{\tilde{\imath}_{L1ref}(s)} = \frac{1}{V_p} \frac{K_P q_2(s)}{p(s)+K_P(N/V_p)q_1(s)} \tag{32}$$

where $1/V_p$ is the transfer function of the PWM modulation circuit. The corresponding characteristic equation is given by

$$p(s) + K_P\,(N/V_p)q_1(s) = 0 \tag{33}$$

The current loop controller is designed to localize the low-frequency dominant pole of the characteristic polynomial at a typical value of $s_{1f} = -3/(RC_2)$. Thus, the required value of *N* can now be obtained using

$$N = \left.\frac{p(s)V_p}{K_P q_1(s)}\right|_{S=-\frac{3}{RC_2}} \tag{34}$$

For K_P = 0.055 and $V_p = 1.5\,V$, the value of *N* obtained is 4. The resulting transfer function $G_{ic}(s) = \tilde{v}_0(s)/\tilde{\imath}_{L1ref}(s)$ is given by

$$G_{ic}(s) = \frac{\tilde{v}_0(s)}{\tilde{\imath}_{L1ref}(s)} = \frac{1.1x10^6\,(s^2 - 870.4s + 8.51x10^6)}{(s+1339)\,(s+2526)\,(s^2+ 989.7s + 2.517x10^6)} \tag{35}$$

The Bode plots of $G_3(s)$ and $G_{ic}(s)$ are shown in Fig. 3a. It should be noted that in the design the controller for the voltage loop (see Fig. 4), $G_{ic}(s)$ is nothing but the open-loop plant. Thus when the current loop with input inductor current is introduced, the resonance peak in the low frequency region is not present in $\tilde{v}_0(s)/\tilde{\imath}_{L1ref}(s)$, which in the design of the voltage loop is the open-loop transfer function. This simplifies the design of the voltage loop.

Next, the conventional PI controller for the voltage loop is considered:

$$G_v(s) = K_{pv} + \frac{K_{Iv}}{s} \tag{36}$$

It is designed with the objective of getting a high gain at the low frequency region to improve the steady-state error performance and to get an overall positive phase margin. For K_{pv} = 0.09, K_{Iv} = 300 and feedback gain K_h = 0.5, the PI controller is given by

$$G_v(s) = \frac{0.09\,s + 300}{s} \tag{37}$$

K_{pv} is designed together with the voltage divider network with gain K_h and the value of $K_{pv}K_h$ is chosen such that the resonance peak at the high frequency region is below 0 dB. The Bode plot of the resulting loop gain $G_L(s)$ (PI controller, voltage divider network and $G_{ic}(s)$) is shown in Fig. 3b. The phase margin achieved is about 77°.

4.3 Controller design using output inductor current

As in the case of input inductor current feedback, the value of K_P is fixed at 0.055 and then the value of N is obtained to localize the low-frequency dominant pole of the characteristic polynomial at a typical value of $s_{1f} = -3/(RC_2)$. Thus, N can be obtained using (34) as

$$N = \left.\frac{p(s)V_p}{K_P q_1{}'(s)}\right|_{S=-\frac{3}{RC_2}} \tag{38}$$

For K_P = 0.055 and $V_p = 1.5\ V$, the value of *N* obtained is 11.

Now, the resulting transfer function $G_{ic1}(s) = \tilde{v}_0(s)/\tilde{\imath}_{L2ref}(s)$ in the case of output inductor current feedback is given as

$$G_{ic1}(s) = \frac{\tilde{v}_0(s)}{\tilde{\imath}_{L2ref}(s)} = \frac{\frac{1}{V_p}*G_c(s)*G_2(s)}{1+\frac{1}{V_p}*G_c(s)*G_2(s)*N} * \frac{G_3(s)}{G_2(s)} = \frac{1}{V_p}\ \frac{K_p q_2(s)}{p(s)+K_p(N/V_p)q_1{}'(s)}$$

$$= \frac{1.1x10^6\ (s^2 - 870.4s + 8.511x10^6)}{(s+1349)\ (s+1152)\ (s^2 - 836.1s + 5.204x10^6)} \tag{39}$$

Note that one of the denominator polynomials of the transfer function, viz., $s^2 - 836.1s + 5.204x10^6$ has a negative coefficient. Thus, the addition of the current loop using the output inductor current leads to an unstable transfer function $G_{ic1}(s)$. However, it is interesting to note that this instability is not easily observed from the Bode plot as the roots (non-minimum phase zeroes) of the numerator polynomial $s^2 - 870.4s + 8.511x10^6$ are almost cancelled by the unstable roots of the denominator polynomial $s^2 - 836.1s + 5.204x10^6$ (see Fig. 5). But, the system is unstable due to the inexact cancellation of unstable poles from the

denominator polynomial. Changing the values of N and K_p does not change the situation and as such it is very difficult to use the output inductor current feedback to get a stable first-order like single dominant pole transfer function $\tilde{v}_0(s)/\tilde{\imath}_{L2ref}(s)$.

The next thing is to investigate whether the current integral control given by $K(s) = K_P + K_I/s$ will change the situation. Previously, for the output inductor current feedback case, $G_c(s) = K_P$ has been used and it resulted in an unstable transfer function. Now, for the input inductor current feedback case, when a current integral action of the form $K(s) = K_P + K_I/s$ is introduced instead of $G_c(s) = K_P$, the transfer function $G_{ic2}(s)$ obtained is given by

$$G_{ic2}(s) = \frac{\tilde{v}_0(s)}{\tilde{\imath}_{L1ref}(s)} = \frac{1}{V_p} \frac{(K_p s+K_I)q_2(s)}{p(s)s+(K_p s+K_I)(N/V_p)q_1(s)} \tag{40}$$

The value of N to localize the low-frequency dominant pole of the characteristic polynomial at a typical value of $s_{1f} = -3/(RC_2)$ is obtained as

$$N = \left.\frac{p(s)*s*V_p}{(K_p s+K_I)q_1(s)}\right|_{s=-\frac{3}{RC_2}} \tag{41}$$

For $K_P = 0.05$ and $K_I = 10$, the value of N obtained is 4.5 and the resulting transfer function $G_{ic2}(s) = \tilde{v}_0(s)/\tilde{\imath}_{L1ref}(s)$ is given by

$$G_{ic2}(s) = \frac{1\times10^6\ (s+200)\ (s^2 - 870.3s + 8.51\times10^6)}{(s+110.4)\ (s^2+ 3846s + 3.9\times10^6)(s^2+ 998.3s + 2.38\times10^6)} \tag{42}$$

The Bode plots of $G_{ic2}(s)$ are shown in Fig. 6. The stable transfer function with no resonance peak in the low frequency region is obtained which simplifies the design of the voltage loop. Thus, for both types of controllers (with and without integral action), input inductor current can be suitably used in feedback to achieve the advantages offered by current-mode control schemes.

However, for the case of the output inductor current feedback, when the PI controller of the form $K(s) = K_P + K_I/s$ is introduced, the transfer function $G_{ic3}(s)$ is given by

$$G_{ic3}(s) = \frac{\tilde{v}_0(s)}{\tilde{i}_{L2ref}(s)} = \frac{1}{V_p} \frac{(K_p s+K_I) q_2(s)}{p(s)s+(K_p s+K_I)(N/V_p) q_1{}'(s)} \quad (43)$$

The value of N to localize the low-frequency dominant pole of the characteristic polynomial at a typical value of $s_{1f} = -3/(RC_2)$ is obtained as

$$N = \left. \frac{p(s)*s*V_p}{(K_p s+K_I) q_1{}'(s)} \right|_{s=-\frac{3}{RC_2}} \quad (44)$$

For $K_P = 0.05$ and $K_I = 10$, the value of N obtained using (44) is 12, and the resulting transfer function $G_{ic3}(s) = \tilde{v}_0(s)/\tilde{\imath}_{L2ref}(s)$ is given by

$$G_{ic3}(s) = \frac{1\times10^7 \ (s+200)\ (s^2 - 870.3s + 8.51\times10^6)}{(s+105.1)\ (s^2+ 2426s + 1.7\times10^6)(s^2-876.9s + 5.16\times10^6)} \quad (45)$$

It is noted that the same unstable pole-zero cancellation is present in the transfer function when the PI controller is designed using the output inductor current for the inner loop. Thus, this again results in an unstable system. The inexact pole-zero cancellation happens for a wide range of values for K_p and K_I. As such, it is very difficult to design the required controller using the output inductor current.

4.4 Further comments

Similar comparison of current mode controllers can be performed for other higher order converters like the cascade boost, Cuk, SEPIC and zeta converters to find the most suitable inductor current for feedback purposes. The main point to note when developing these controllers is to use only the output voltage and one inductor current for feedback. Further procedure for comparison of the controllers follows the approach described in sections 2, 3 and 4. To avoid repetition, this will not be covered in this paper. Secondly, it is also important to note that the scope of this paper is limited to the CCM operation. For the DCM case, the approach of comparison will be same, but the state space model and transfer functions will be different.

5 Experimental Results

A laboratory prototype of the POEL converter was built to validate the results for the current-mode controllers. Eq. (7) is implemented using simple analog components. The following circuit parameter values were used for experimental work:

$$E = 5V,\ L_1 = 1mH,\ L_2 = 10mH,\ C_1 = 47\mu F,\ C_2 = 100\mu F$$

The switching frequency used was 20 kHz and $V_p = 1\,V$. No filtering of signals was carried out.

Fig. 7(a) shows the output response of the converter when a step reference voltage $V_d = 6\,V$ was applied. Here, $K_{p1} = 0.07$ and $K_{I1} = 3.3$ were used. Fig. 7(b) shows the output response when reference is changed back to 0V. Fig. 7(c) shows the output response in the presence of a load change from $R = 1k\Omega$ to $R = 666\,\Omega$ (33.3 % reduction) and then back to $R = 1k\Omega$. An overshoot of approximately 0.4V and a settling time of around 400 ms is observed. Fig. 7(d) shows the output response in the presence of a load change from $R = 1k\Omega$ to $R = 500\Omega$ (50 % reduction) and then back to $R = 1k\Omega$. A comparatively high overshoot (of approx. 0.8V) is observed with small steady state error of approximately 0.2 V. Such deviation from the ideal behavior is expected since the current-mode controller is designed using the linearized model of the POEL converter which is valid only in the neighborhood of specific operating point. This is the limitation of the paper.

Next, the variation in the output response for various values of controller gain is studied. Fig. 8(a) shows the transient output response for $K_{p1} = 0.03$ and $K_{I1} = 0.7$. An overshoot of approximately 0.6 V is observed and the settling of 200 ms is obtained. Figs. 8(b) to 8(d) shows the output voltage response for a load change from $R = 1k\Omega$ to $R = 666\,\Omega$ and then back to $R = 1k\Omega$ for $K_{I1} = 4$, 3.32 and 2.3 respectively and using $K_{p1} = 0.07$. Steady state control signal to the gate terminal of the MOSFET is shown in Fig. 9. All these results show

that the controller using the input inductor current is suitable for the regulation of the POEL converter.

6 Conclusions

This paper has presented a comparative study of current-mode controllers for the POEL converter using the input and output inductor currents. Both the state-space and frequency response approaches were used to gain a better insight into the comparative study. From the results, it is seen that the controller using the output inductor current is not a very good choice for feedback purposes. It appears that in the state-space case, even for small controller gains, the closed-loop system is unstable, whereas in the frequency response case, the incorporation of a current loop using the output inductor current leads to unstable pole-zero cancellations. It is also shown that such instability is not easily observed from the Bode plot. On the other hand, it is also shown that the two types of stable controllers implemented (with and without integral action) using the input inductor current for feedback provides a wide range of controller parameters for tuning. This resulted in the elimination of the resonance peak and thus increasing the system bandwidth. As such the input inductor current is found to be more suitable for feedback purposes.

7 References

1 Tseng, C., Liang, T.J.: 'Novel high efficiency step-up converter', *IEE Proc. Electr. Power Appl*., 2004, **151**, (2), pp. 182-190

2 Abutbuli, O., Gherlitz, A., Berkovich, Y., Ioinovici, A.: 'Step-up switching-mode converter with high voltage gain using a switched-capacitor circuit', *IEEE Trans. Circuits Syst.* I, 2003, **50**, (8), pp. 1098-1102

3 http:/www.researchandmarkets.com

4 Ahmed, O. A, Bleijs, J.A.M.: 'High-efficiency DC-DC converter for fuel cell, applications: Performance and dynamic Modelling', *ECCE2009*, San Jose, USA, 2009, pp. 67-74

5 Sharma, R., Gao, H.: 'Low cost high efficiency DC-DC converter for fuel cell powered auxiliary power unit of a heavy vehicle', *IEEE Trans. Power Electron.*, 2006, **21**, (3), pp. 587 - 591

6 Jain, S., Jiang Jin, Huang Xinhong, Stevandic, S.: 'Modeling of fuel-cell-based power supply system for grid interface', IEEE *Trans. Ind. Appl.*, 2012, **48**, (4), pp. 1142 – 1153

7 Luo, F.L.: 'Luo converters–voltage lift technique', *Proc. IEEE Power Electronics Special Conf.*, 1998, pp. 1783–1789

8 Luo, F.L.: 'Positive output Luo converters: voltage lift technique', *IEE Proc. Electr. Power Appl.*, July, 1999, **146**, (4), pp. 415-432

9 Luo, F.L., Ye, H.: 'Positive output super lift converters', *IEEE Trans. Power Electron.*, 2003, **18**, (1), pp. 105–113

10 Luo, F.L., Ye, H.: 'Negative output super lift converters', *IEEE Trans. Power Electron.* 2003, **18**, (5), pp. 1113–1121

11 Luo, F.L., Ye, H.: 'Energy Factor and Mathematical Modeling for Power DC/DC Converters', *IEE Proc. Electr. Power Appl.,* March 2005, **152**, (2), pp. 191-198

12 Luo, F.L., Ye, H.: 'Ultra-lift Luo-converter', *IEE Proc. Electr. Power Appl.*, Jan. 2005, **152**, (1), pp. 27–32

13 Luo, F.L., Ye, H.: 'Advanced DC/DC converters' (Boca Raton: CRC Press, 2004)

14 He, Y., Luo, F.L.: 'Sliding-mode control for dc-dc converters with constant switching frequency', 2006, *IEE Proc. Control Theory Appl.*, **153**, (1), pp. 415-432.

15 Ravichandran, S., Patnaik, S.K.: 'Implementation of dual-loop controller for positive output elementary Luo converter', *IET Power Electron.*, 2013, **6**, (5), pp. 885 – 893,

16 Chan, C.Y.: 'Comparative study of current-mode controllers for a high-order boost dc-dc converter', *IET Power Electronics*, 2014, **7**, (1), pp. 237-243

17 Dixon, L. H.: 'Average current mode control of switching power supplies', Unitrode Power Supply Design Seminar Handbook, 1997

18 Yang, Z.H., Sen, P.C.: 'DC-to-DC buck converters with novel current mode control', *Proc. IEEE Power Electron. Spec. Conf.*, 1999, pp. 1158 – 1164

19 Deisch, C. W.: 'Switching control method changes power converter into a current source', in *Proc. IEEE Power Electron. Spec. Conf.*, 1978, pp. 300–306

20 Chattopadhyay, S., Das, S.: 'A digital current-mode control technique for DC–DC converters', *IEEE Trans. Power Electron.*, 2006, **21**, (6), pp. 1718 – 1726

21 Liu, Y.F., Meyer, E., Liu, X.D.: 'Recent developments in digital control strategies for DC/DC switching power converters', *IEEE Trans. Power Electron.*, 2009, **24**, (11), pp. 2567 – 2577

22 Leyva-Ramos, J., Ortiz-Lopez, M.G., Diaz-Saldierna, L.H., Martinez-Cruz, M.: 'Average current controlled switching regulators with cascade boost converters', *IET Power Electron.* , 2011, **4**, (1), pp. 1-10

23 Khalil, H.: 'Nonlinear systems' (3rd ed. Saddle River, NJ: Pearson Educational International, 2000)

24 Ogata, K.: 'Modern control engineering' (3rd ed. Upper Saddle River, NJ: Prentice-Hall, 1997)

25 Morales-Saldaña, J.A., Loera-Palomo, R., Palacios-Hernández, E., González-Martínez, J.L.: 'Modelling and control of a DC-DC quadratic boost converter with R^2P_2', *IET Power Electronics*, 2014, **7**, (1), pp. 11-22

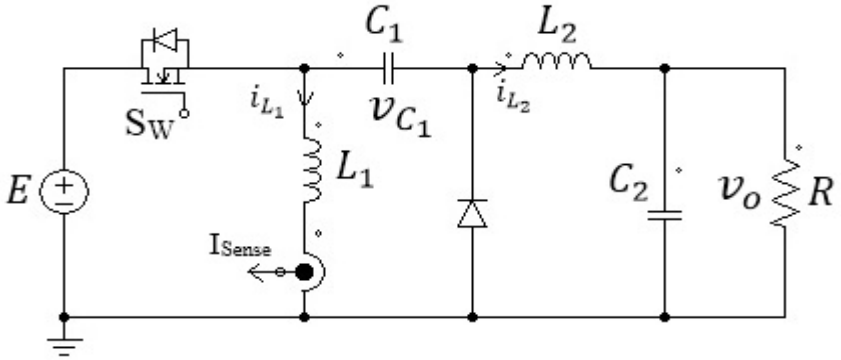

Fig. 1 *Circuit diagram of the POEL converter*

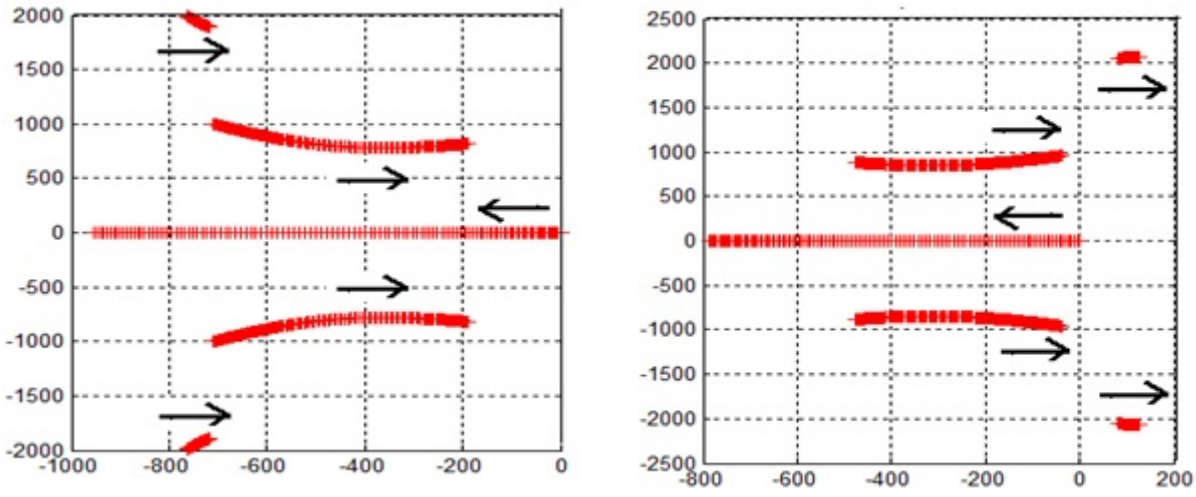

(a) (b)

Fig. 2 Root locus plot for $K_{P1} = 0.08$, $0 < K_{I1} < 12$
(a).using input inductor current feedback *(b).* using output inductor current feedback

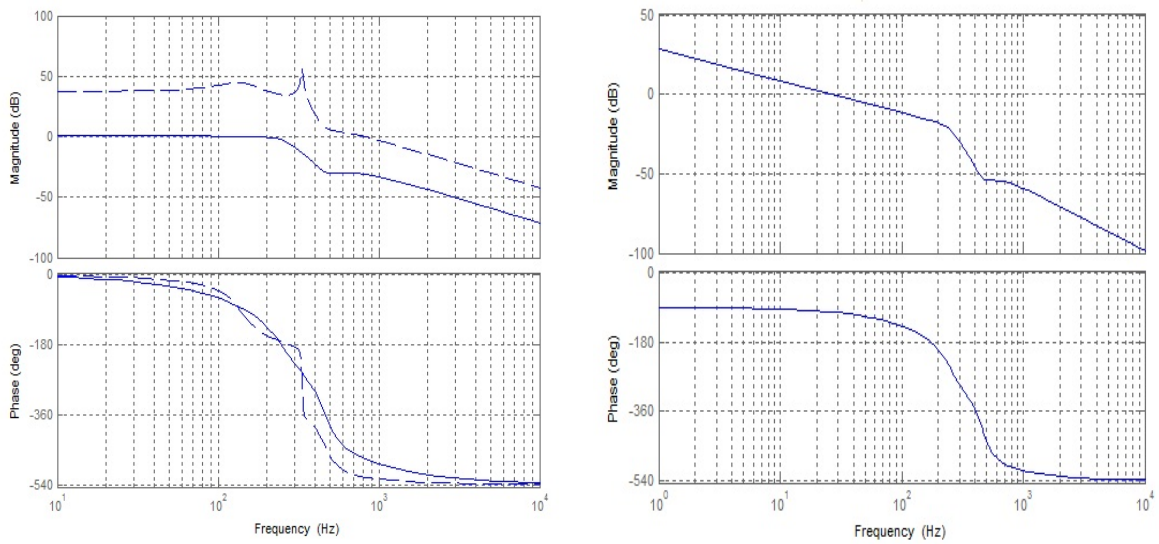

(a) *(b)*

Fig. 3 *Bode plots using input inductor current feedback*
(a). Bode plots of $G_3(s)$ *(dotted) and* $G_{ic}(s)$ *(Solid)*
(b). Bode plot of loop gain $G_L(s)$

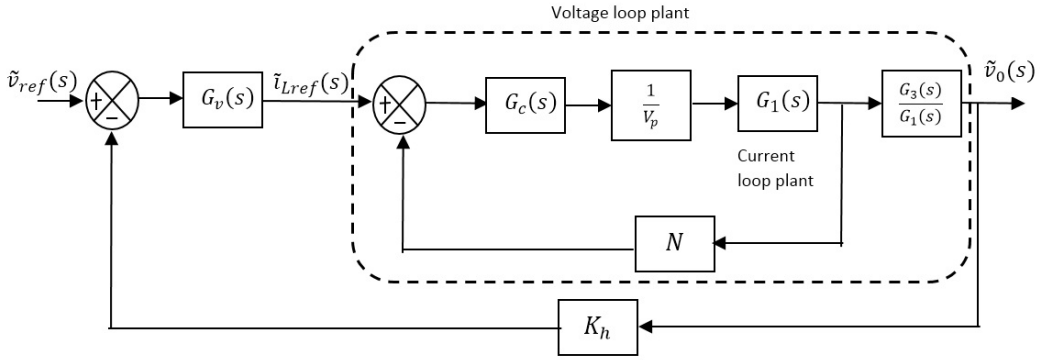

Fig. 4 *Multi-loop controller scheme*

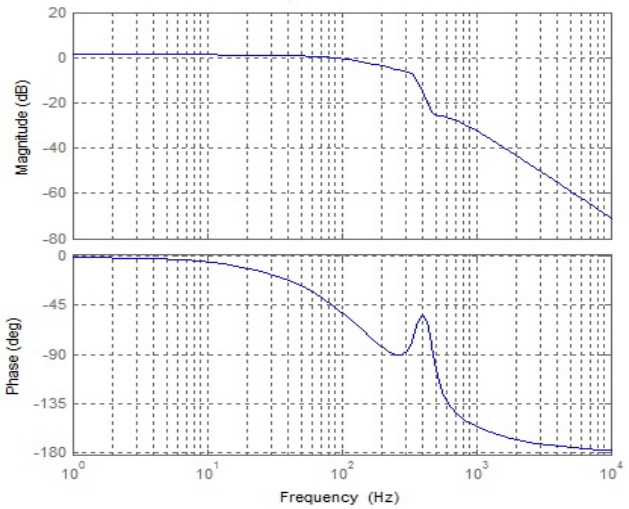

Fig. 5 *Bode plot of* $G_{ic1}(s)$
(using output inductor current feedback)

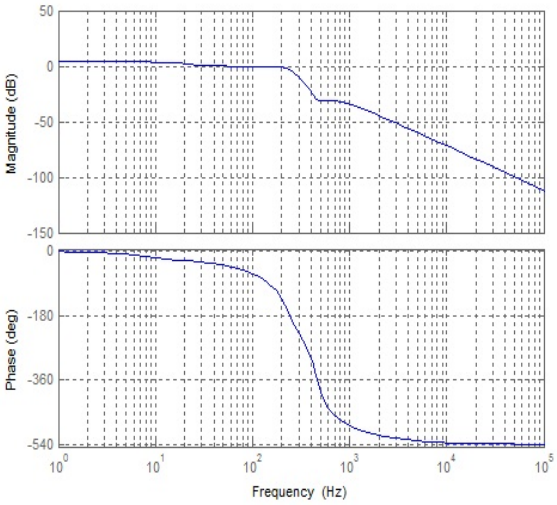

Fig. 6 *Bode plot of loop gain* $G_{ic2}(s)$
(using input inductor current feedback)

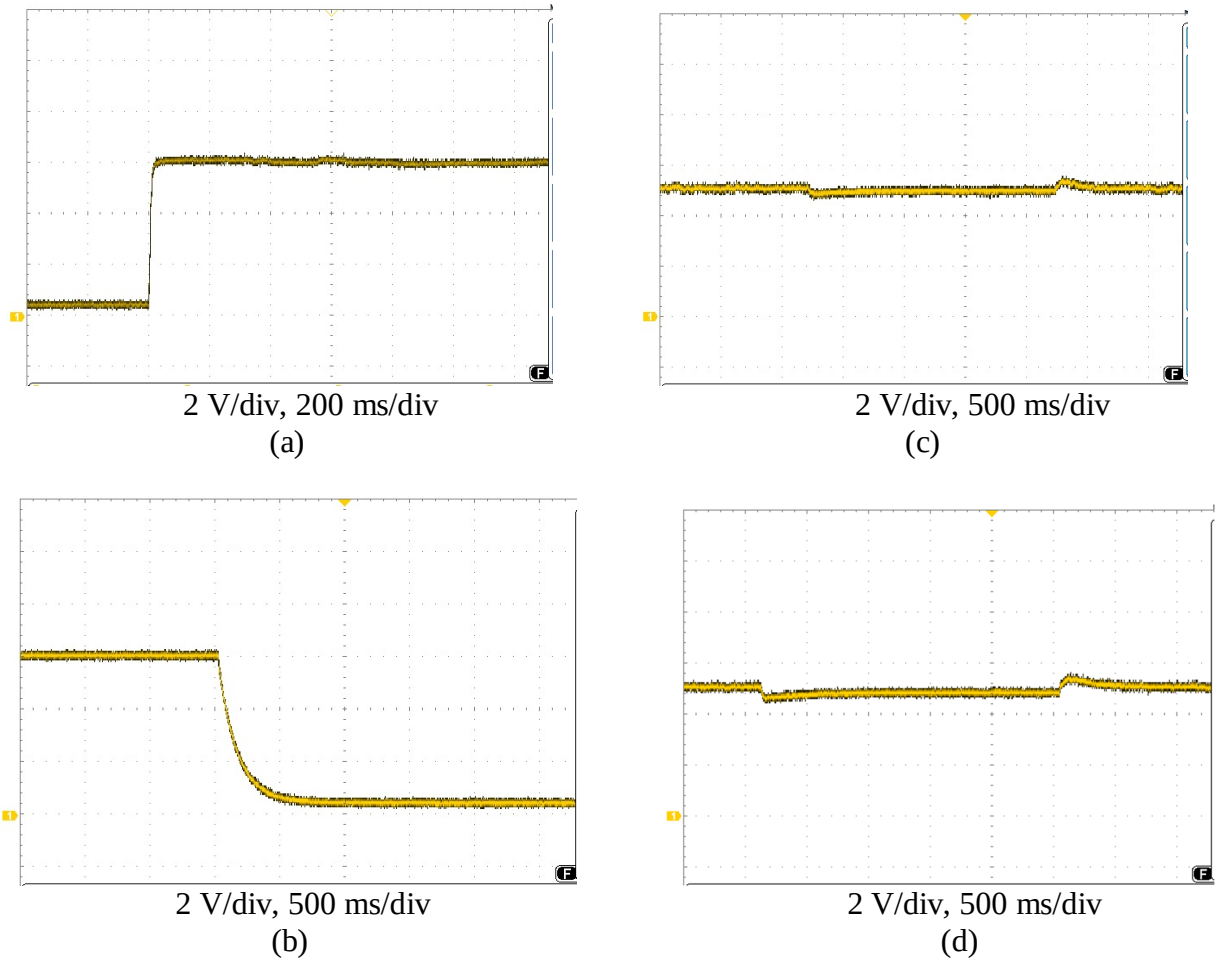

Fig. 7 *System response using* $K_{p1} = 0.07$ and $K_{I1} = 3.3$

(a). Transient Output response (0 to 5 V)
(b). Transient Output response (5 to 0 V)
(c). Output response in the presence of load change ($R = 1k\Omega$ to $R = 666\ \Omega$)
(d). Output response in the presence of load change ($R = 1k\Omega$ to $R = 500\ \Omega$)

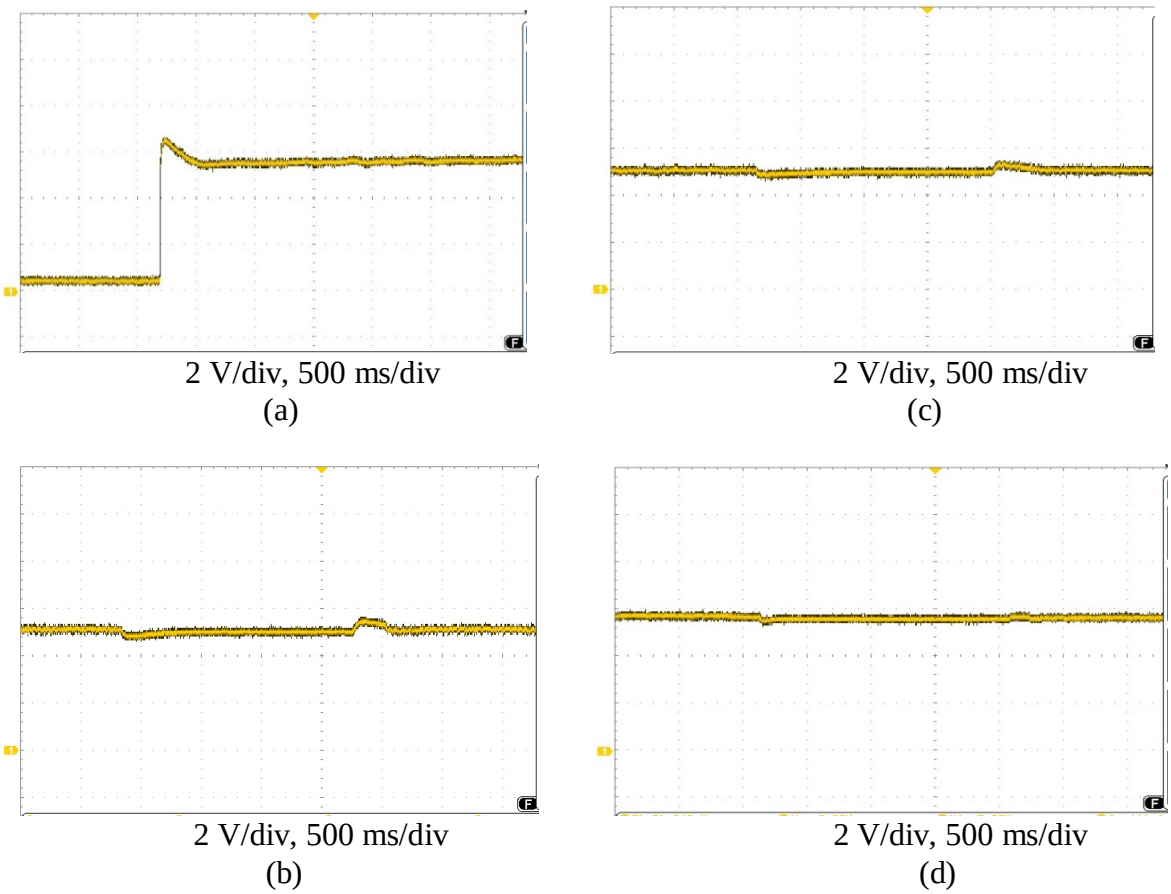

2 V/div, 500 ms/div
(a)

2 V/div, 500 ms/div
(c)

2 V/div, 500 ms/div
(b)

2 V/div, 500 ms/div
(d)

Fig. 8 *System response using different values of controller gains*

(a). Transient Output response ($K_{p1} = 0.03$, $K_{I1} = 0.7$)

(b). Output response using load change ($R = 1k\Omega$ to $R = 666\ \Omega$ for $K_{I1} = 4, K_{p1} = 0.07$)

(c). Output response using load change ($R = 1k\Omega$ to $R = 666\ \Omega$ for $K_{I1} = 3.3, K_{p1} = 0.07$)

(c). Output response using load change ($R = 1k\Omega$ to $R = 666\ \Omega$ for $K_{I1} = 2.3, K_{p1} = 0.07$)

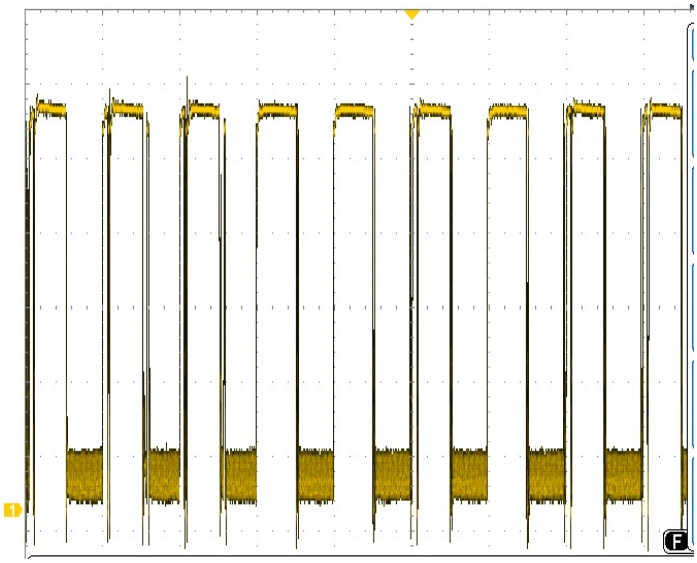

2 V/div, 50 us/div

Fig. 9 Steady state control signal to the gate terminal of the MOSFET